JOURNAL OF MATERIALS SCIENCE 21 (1986) 1310–1320

Metastable MC phase in melt-quenched Fe–C–V and Fe–C–V–(Cr or Mo) alloys – mechanical properties and powder-forming tendency by comminution

A. INOUE, Y. HARAKAWA*, M. OGUCHI*, T. MASUMOTO
The Research Institute for Iron, Steel and Other Metals, Tohoku University, Sendai 980, Japan

A metastable fcc MC phase has been found in Fe–C–V ternary and Fe–C–V–Cr and Fe–C–V–Mo quaternary alloys quenched rapidly from the melts. The formation of the MC single phase is limited to the range 12 to 20 at% C and above 10 at% V for Fe–C–V alloys and above 19 at% V and below 12 at% Cr for Fe–18% C–V–Cr alloys. The MC phase is an iron-rich and carbon-poor solid solution of stable VC phase which was formed by the suppression of the equilibrium reaction from liquid to ferrite + VC, and the lattice parameter increases almost linearly from 0.4048 to 0.4147 nm with increasing carbon, vanadium. chromium and molybdenum contents. The MC phase possesses a highly brittle nature combined with hardness as high as about 700 to 1200 DPN and hence is readily comminuted into irregularly polygonal powders of a desirable size range below 325 mesh (44 μm) by a hammer milling treatment. Annealing at temperatures above 973 K results in the decomposition of the MC phase into an aggregate of stable ferrite, including a uniform dispersion of fine VC carbide accompanied by a remarkable reduction in hardness and a significant increase in ductility. It is therefore said that the resulting Fe–C–V and Fe–C–V–X (X = chromium or molybdenum) powders dissolving carbon, vanadium and chromium (or molybdenum) by as much as about 25 to 40 at%, are highly attractive as raw materials for consolidation into bulk form by conventional powder consolidation techniques, owing to the expectation that their bulk material exhibits higher strengths and better ductility compared to those of the alloys solidified in the usual manner.

1. Introduction

For the last several years, Inoue and co-workers have presented a series of results concerning the effect of melt-quenching on the microstructures and mechanical properties of Fe–C–X (X = chromium, molybdenum, tungsten, aluminium or silicon) alloys containing ferrite-forming X elements [1–7]. It has been clarified in their presentations that various kinds of metastable phases such as amorphous, chi (χ), epsilon (ε), austenite (γ), martensite (α'), kappa (κ) and cementite (M_3C) are formed in the Fe–C–X systems and the amorphous [1, 2] and austenite [4–6] phases have a high level of strength as well as good ductility, even though the other metastable phases exhibit an extremely brittle nature. These results indicate that the melt-quenching technique is very useful to bring solid solutions, which are stable only at high temperatures, to an ambient temperature region through the suppression of equilibrium phase reactions into α (or α') + alloy carbides, etc.

We have subsequently examined the melt-quenched structures of Fe–C–V, Fe–C–V–Cr and Fe–C–V–Mo alloys containing vanadium, which belongs to the same ferrite-forming group, because of the high engineering potential of the vanadium-containing alloys. Furthermore, considering the facts that the lattice parameter of VC carbide is the smallest ($\simeq$ 0.416 nm) [8] among equilibrium MC-type carbides, and is larger only by 15% than that of austentic (γ) pure iron, in addition to a similarity of crystalline structure between VC and γ-iron, the solid solution of γ-iron and/or VC is expected to be formed in remarkably extended composition ranges in melt-quenched Fe–C–V, Fe–C–V–Cr and Fe–C–V–Mo alloys. The supersaturated solid solution containing large amounts of carbon and vanadium is expected to be practically used as a raw material to produce a lath-martensite alloy with finely dispersed VC carbide upon subsequent annealing. Accordingly, investigations of the formation of the supersaturated solid solution of γ-iron and/or VC phases and its decomposition behaviour are very attractive from engineering and scientific points of view. This paper intends to present (1) the composition range in which the extended solid solution of γ-iron or VC phase is formed in Fe–C–V ternary and Fe–C–V–Cr and

Permanent address: Research and Development Department, Teikoku-Piston Ring Ltd, Okaya 394, Japan.

0022–2461/86 $03.00 + .12 © *1986 Chapman and Hall Ltd.*

Fe–C–V–Mo quaternary systems, (2) the microstructure, mechanical properties and powder-forming tendency of the metastable solid solution, and (3) the changes in its structure and mechanical properties upon annealing.

2. Experimental procedure

The specimens used in the present work are Fe–C–V ternary and Fe–C–V–Cr and Fe–C–V–Mo quaternary alloys. Mixtures of pure metals (iron, vanadium, chromium and molybdenum), white cast iron and graphite were melted under an argon atmosphere in an induction furnace to prepare the master alloys. The melts were sucked up into quartz tubes of about 3 mm inner diameter and solidified in the tubes. The compositions were determined by the nominal values in atomic per cent since the difference between nominal and chemically analysed compositions is less than 0.08 wt % for carbon, 0.3 wt % for vanadium, 0.6 wt % for chromium and 0.5 wt % for molybdenum. From these master alloys, long ribbons of about 1 mm width and 20 μm thickness were prepared by a single roller melt-spinning apparatus as the samples for examining structure, hardness and powder-forming tendency. The amount of melted alloys per run was about 10 g and the rotation speed of the steel roll (20 cm diameter) was controlled at about 6000 r.p.m. Additionally, a continuous wire of about 100 μm diameter was prepared by melt spinning in rotating water as the sample for measuring tensile strengths and elongation.

As-quenched structures of the specimens were examined by optical and transmission electron microscopies and X-ray diffraction using Cu$K\alpha$ radiation in combination with an X-ray monochromator. The transmission electron microscopy (TEM) specimens were prepared by electrical thinning of ribbon in a solution of 10% by volume perchloric acid in methanol immersed in iced water. The optical microscope samples were prepared by chemical etching of the polished surface in a solution of 5% by volume nitric acid in methanol at room temperature. The hardness and tensile strengths were measured by a Vickers microhardness tester with a 50 g load and an Instron-type tensile testing machine at a strain rate of $1.7 \times 10^{-4}\,\mathrm{sec}^{-1}$. Tensile specimens were cut from annealed long wires into the short wires having a gauge dimension of 20 mm. A specially designed set of grips for the wire specimens was used to ensure proper specimen alignment within the machine. In order to evaluate a powder-forming tendency of the melt-quenched phases, the ribbon samples were comminuted at room temperature for 30 min by using a hammer milling apparatus. The classification of the comminuted powders was made by sieving the powders using screens of different mesh sizes. The tensile fracture surface morphology of the wires and the shape and surface structure of the sieved powders were observed by scanning electron microscopy.

3. Results and discussion

3.1. Melt-quenched structure for Fe–C–V alloys

The compositional dependence of melt-quenched structures in Fe–C–V ternary alloys is shown in Fig. 1a, along with the equilibrium phase diagram at 973 K (Fig. 1b) [9]. The open circles shown in Fig. 1a represent the alloy compositions that were examined. Single-phase fields of martensite (α'), MC and M_3C, two-phase fields of α' + MC, ferrite (α) + MC, γ + MC, and γ + M_3C and a three-phase fields of γ + α' + M_3C are outlined in the diagram. However, the location of their boundaries is somewhat arbitrary because the composition of the ejected alloys has an interval of about 5 at % V and 2 at % C. As shown in Fig. 1a, no amorphous phase was formed in this alloy system. As is evident from comparison of Figs. 1a and b, the MC in their melt-quenched phases is concluded to be a metastable phase found for the first time in the present investigation. The formation of the MC single phase is limited to the range of about 11 at % C and above about 10 at % V. Additionally, the melt-quenching causes a remarkable extension of the solid solubility of carbon in ferrite from 1 at % C at 973 K in an equilibrium state to about 7 at % C, accompanied by the formation of martensite phase. Here, it may be necessary to keep in mind that the formation ranges of the α', α, MC and M_3C change significantly with cooling rate during and after solidification and the type of melt-quenching technique used.

The typical microstructure of the MC single phase in $Fe_{60}C_{20}V_{20}$ alloy is shown in Fig. 2, where (a) is a bright-field image, and (b) is the selected-area diffraction pattern in (a). In (b), the appearance of the reflection rings of 1 1 1, 0 0 2 and so forth indicates clearly that the phase has an f c c structure which is the same as the VC carbide. The MC phase consists of grains as fine as about 40 nm and a high density of internal

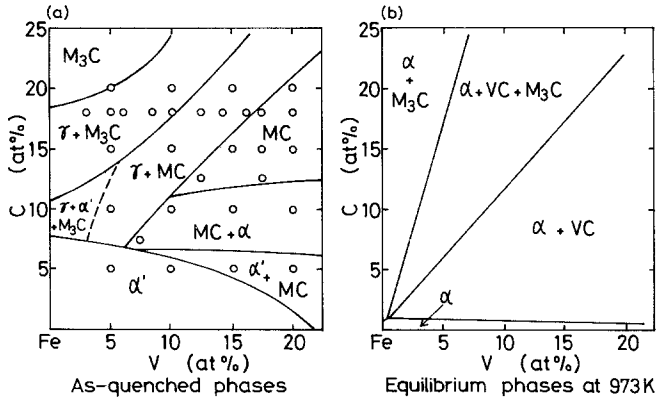

Figure 1 (a) Melt-quenched phases and (b) equilibrium phases at 973 K in Fe–C–V ternary system.

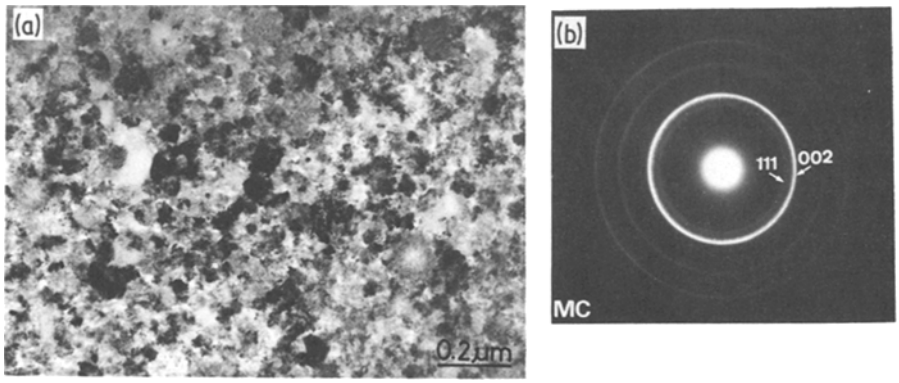

Figure 2 (a) Transmission electron micrograph and (b) selected-area diffraction pattern showing the fcc (Fe, V)C phase in a melt-quenched Fe–20C–20V alloy.

faults are seen within the grains. The lattice parameter of the MC phase in melt-quenched $Fe_{100-2x}V_xC_x$ alloys determined from the X-ray diffraction analysis increases almost linearly with increasing carbon and vanadium contents, e.g. from 0.4048 nm at $x = 10$ at % to 0.4074 nm at $x = 20$ at % as shown in Fig. 3. These values are much smaller than that of stable VC ($a \simeq 0.414$ nm) [8] because of the dissolution of much smaller amounts of carbon and vanadium. If one allows extrapolation of the linear relation presented in Fig. 3, up to the stoichiometric value of VC, the lattice parameter of the hypothetical VC phase is evaluated to be about 0.415 nm, being nearly the same as that (0.414 nm) [8] of VC. Considering the previous results [1–3] that the amorphous phase formation in Fe–C–X (X = chromium, molybdenum, tungsten) alloys is located in the range of 14 to 22 at % C and above about 6 at % X, the amorphous phase formation was also expected in the composition range in which the MC phase is formed. Nevertheless, no trace of amorphous phase was found at all compositions in the Fe–C–V alloys examined in the present work. Although the reason why no amorphous phase was formed in the Fe–C–V system remains uncertain at present, it may be due to a strong formation tendency of the MC-type carbide. This inference is supported from the result that the composition range, where the amorphous phase formation is expected, is included in the formation range of the MC phase.

Fig. 4 shows the change in the microstructures of $Fe_{80-x}C_{20}V_x$ alloys with vanadium content. The melt-quenched phases of $Fe_{75}C_{20}V_5$ and $Fe_{70}C_{20}V_{10}$ alloys consist mainly of M_3C phase containing numerous internal faults and the grain size of the M_3C phase decreases significantly with increasing vanadium content. The further increase in vanadium content results

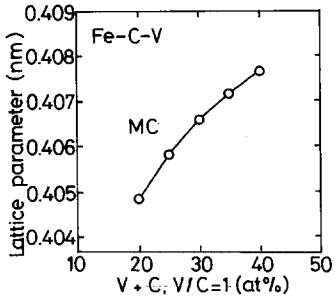

Figure 3 Variation of lattice parameter of fcc (Fe, V)C phase in Fe–C–V alloys as a function of V + C (V/C = 1) content.

in the phase transition of M_3C to MC accompanied by a further increase in the density of internal faults. Such a change in the microstructure is thought to occur for the reduction of large internal strain generated by the dissolution of a large amount of vanadium. The feature of the duplex MC + γ structure in $Fe_{65}C_{20}V_{15}$ alloy is very similar to that of the MC single phase in $Fe_{60}C_{20}V_{20}$ alloy shown in Fig. 2. Thus, the increase in vanadium content causes an enhancement of the formation tendency of the MC solid solution. Such a systematic change in the as-quenched structure for the series of $Fe_{80-x}C_{20}V_x$ alloys indicates that the cooling rate during and after solidification increases with increasing vanadium content in the range below 20 at %.

Fig. 5 shows the change in the melt-quenched structure of $Fe_{80-x}C_xV_{20}$ alloys with carbon content. The melt-quenched $Fe_{75}C_5V_{20}$ alloy is composed of lath martensite (α'_L) including the MC carbide with a size as fine as about 20 nm. As the carbon content increases, the amount and size of the MC precipitates increase significantly accompanied with the phase transition from α'_L to ferrite (α) because the phase change ($\alpha' \rightarrow \alpha$) of the matrix causes a significant reduction in the solid solubility limit of carbon. A further increase in carbon content from 10 to 20 at % results in a remarkable increase in cooling rate during solidification owing to the great supercooling ability of the liquid containing metalloid content nearly comparable to a eutectic composition, leading to the formation of metastable MC single phase having iron-rich and carbon-poor compositions. The melt-quenched phase diagram shown in Fig. 1a allows us to expect that the formation range of the metastable MC phase may be extended into a further carbon- and/or vanadium-rich composition region, but melt-quenched ribbons of the Fe–C–V alloys containing above 20 at % C and 20 at % V could not be prepared because of their melting temperatures higher than about 1800 K [10].

3.2. Melt-quenched structures of Fe–18% C–V–Cr and Fe–18% C–V–Mo alloys

It has been demonstrated previously [1–3] that the addition of chromium and/or molybdenum into Fe–C alloys results in a remarkable extension of the formation range of the amorphous phase because of the lowering of melting temperature (T_m) and the rise of glass transition temperature (T_g) caused by an

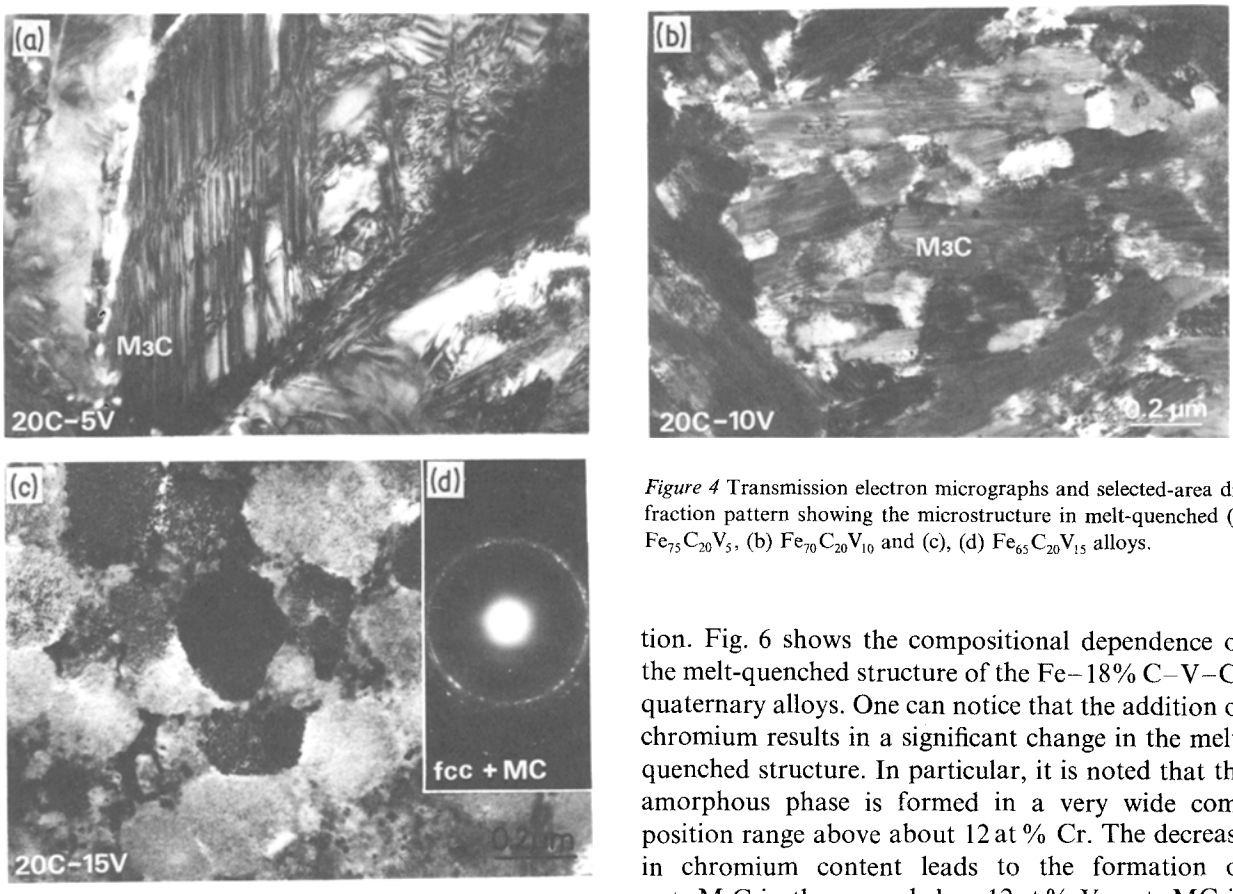

Figure 4 Transmission electron micrographs and selected-area diffraction pattern showing the microstructure in melt-quenched (a) $Fe_{75}C_{20}V_5$, (b) $Fe_{70}C_{20}V_{10}$ and (c), (d) $Fe_{65}C_{20}V_{15}$ alloys.

enhancement in an attractive interaction between the metal and metalloid atoms in their liquid [11, 12]. This may permit one to expect that the application of melt-quenching to Fe–C–V–Cr and Fe–C–V–Mo alloys causes the formation of an amorphous phase or a further extension of the metastable MC solid solution. Fig. 6 shows the compositional dependence of the melt-quenched structure of the Fe–18% C–V–Cr quaternary alloys. One can notice that the addition of chromium results in a significant change in the melt-quenched structure. In particular, it is noted that the amorphous phase is formed in a very wide composition range above about 12 at % Cr. The decrease in chromium content leads to the formation of $\gamma + M_3C$ in the range below 12 at % V, γ + MC in the range from 10 to 22 at % V and MC single phase in the vanadium-rich range above about 20 at % V. As an example, Fig. 7 shows the microstructure of MC single phase in melt-quenched $Fe_{57}C_{18}V_{20}Cr_5$ alloy. The grain is as fine as about 0.1 to 0.2 μm and contains an extremely high density of internal faults. Furthermore, it is important to note that no detectable

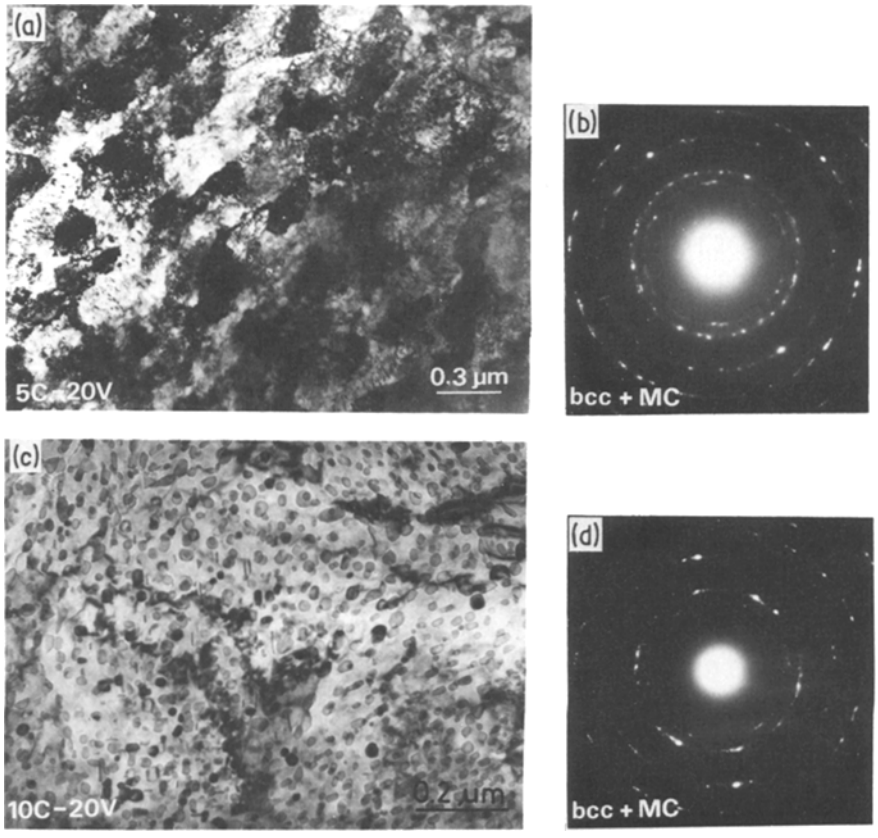

Figure 5 Transmission electron micrographs and selected-area diffraction patterns showing the microstructure in melt-quenched (a), (b) $Fe_{75}C_5V_{20}$ and (c), (d) $Fe_{70}C_{10}V_{20}$ alloys.

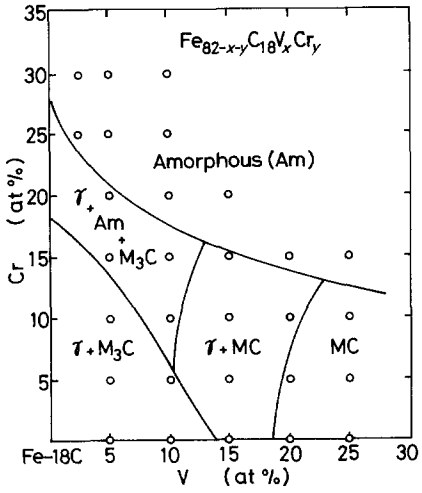

Figure 6 Melt-quenched phases in $Fe_{82-x-y}C_{18}V_xCr_y$ alloys. Open circles represent the alloy compositions that were examined.

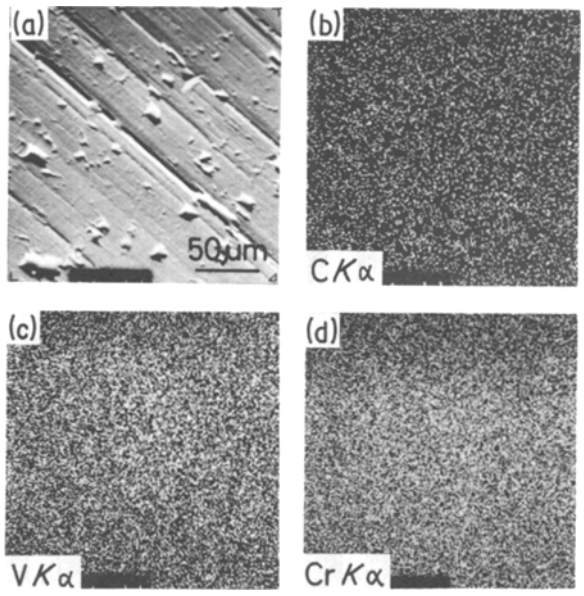

Figure 8 (a) Scanning electron micrograph showing the surface state of melt-quenched $Fe_{56}C_{14}V_{15}Cr_{15}$ ribbon and X-ray images showing the distribution of (b) carbon, (c) vanadium and (d) chromium.

segregation of the constituent elements on the scale of $\simeq 1\,\mu$m is observed because the structure of the melt-quenched ribbon is composed of the MC single phase, evidence for which is seen in Fig. 8 revealing the X-ray images of the constituent elements (carbon, vanadium and chromium).

A similar MC single phase was formed in melt-quenched $Fe_{57}C_{18}V_{20}Mo_5$ alloy as shown in Fig. 9. The comparison of Figs. 7 and 9 indicates that the grain size of the MC phase in the Fe–C–V–Mo alloy is smaller by a factor of about 2 to 3 than that in the Fe–C–V–Cr alloy, and the continuity of their electron diffraction rings is greater for the Fe–C–V–Mo alloy. From such a difference in the melt-quenched structure, the supercooling ability for the Fe–C–V–Mo alloy is inferred to be considerably higher than that for the Fe–C–V–Cr alloy, similar to the tendency [1, 3] for Fe–C–Cr and Fe–C–Mo alloys. This is probably because an attractive interaction among the constituent atoms is stronger for the Fe–C–V–Mo alloy than for the Fe–C–V–Cr alloy.

Fig. 10 shows the lattice parameter of the MC phase in melt-quenched $Fe_{62-x}C_{18}V_{20}Cr_x$ and $Fe_{62-x}C_{18}V_{20}Mo_x$ alloys as a function of chromium or molybdenum content. The lattice parameter increases with increasing chromium or molybdenum content, e.g. from 0.4071 nm for $Fe_{57}C_{18}V_{20}Cr_5$ to 0.4080 nm for $Fe_{47}C_{18}V_{20}Cr_{15}$ and from 0.4115 nm for $Fe_{57}C_{18}V_{20}Mo_5$ to 0.4147 nm for $Fe_{52}C_{18}V_{20}Mo_{10}$. Thus, the lattice parameter is considerably larger for the Fe–C–V–Mo alloys and the increase in the lattice parameter of the MC phase per 1 at % chromium or molybdenum addition is larger by a factor of 1.8 for molybdenum. This is probably because the atomic size of molybdenum is larger by about 9.4% than that of chromium [13].

3.3. Hardness of the MC phase

The Vickers hardness (H_v) of the metastable MC and MC + α phases is plotted as a function of vanadium + carbon content for $Fe_{100-2x}C_xV_x$ alloys in Fig. 11 and as a function of chromium or molybdenum content for $Fe_{62-x}C_{18}V_{20}Cr_x$ and $Fe_{62-x}C_{18}V_{20}Mo_x$ alloys in Fig. 12. H_v increases almost linearly from 530 DPN at $x = 7\%$ to 1150 DPN at $x = 20\%$ for the Fe–C–V alloys and from 1015 DPN at $x = 0\%$ to 1190 DPN at $x = 15\%$ for the Fe–C–V–Cr alloys, and to 1200 DPN at $x = 10\%$ for the Fe–C–V–Mo alloys. It is thus noted that the metastable MC phase possesses hardness as high as about 700 to 1200 DPN. The high hardness level is considered to originate from the solid solution hardening due to carbon, vanadium, chromium and molybdenum and the strengthening by the refinement of grain size and by the introduction of a high density of internal faults. Furthermore, the hardness of a stoichiometric VC carbide is estimated to be about 3300 DPN from a linear extrapolation of the data shown in Fig. 11. The extrapolated hardness value is higher by about 500 DPN than the previously

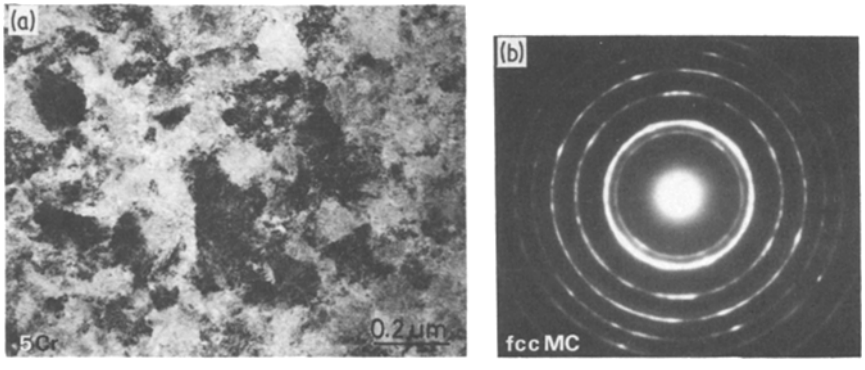

Figure 7 (a) Transmission electron micrograph and (b) selected-area diffraction pattern showing the fcc (Fe, V, Cr)C phase in a melt-quenched $Fe_{57}C_{18}V_{20}Cr_5$ alloy.

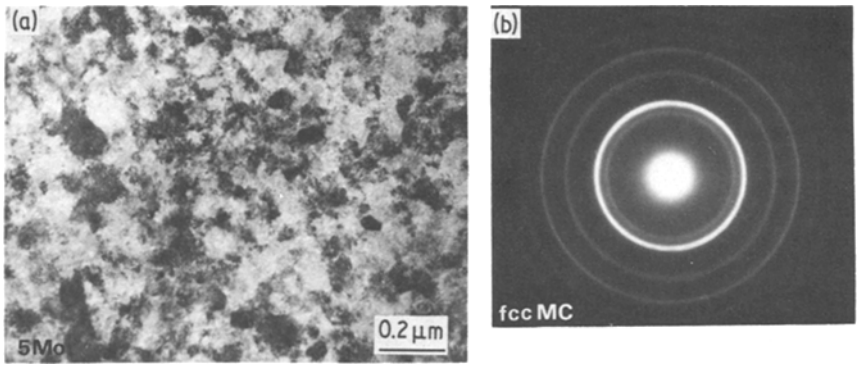

Figure 9 (a) Transmission electron micrograph and (b) selected-area diffraction pattern showing the fcc (Fe, V, Mo)C phase in a melt-quenched $Fe_{57}C_{18}V_{20}Mo_5$ alloy.

reported value ($\simeq$2800 DPN) [14] of VC, and the reason for the difference is probably because the hardness value extrapolated from the data on the metastable MC phase includes the additional contributions of the strengthenings due to the grain size refinement and the existence of a high density of internal faults.

3.4. Comminution tendency of the MC phase ribbon to powder

The ribbon samples of the metastable MC phase in Fe–C–V, Fe–C–V–Cr and Fe–C–V–Mo alloys were comminuted for 30 min by hammer milling in order to evaluate its comminution tendency to powder. As an example, Fig. 13 shows the distribution of powder size of $Fe_{56}C_{14}V_{15}Cr_{15}$ alloy having the metastable MC single phase. More than about 87% of the powders have sizes smaller than 44 μm. A similar distribution of powder size was also recognized for the MC phase in $Fe_{60}C_{20}V_{20}$ and $Fe_{52}C_{18}V_{15}Mo_{15}$ alloys and the MC phase ribbons are concluded to possess a good comminuted tendency to fine powder by the hammer milling treatment. The shape and surface structure of the communited $Fe_{56}C_{14}V_{15}Cr_{15}$ powders are shown in Fig.14. The powder morphology is that of irregularly shaped polygons and no distinct trace of the original ribbon shape is seen. Thus, the melt-quenched ribbons consisting of MC single phase can be easily pulverized into powders of a desirable size range below 325 mesh (44 μm).

3.5. Structural change in the MC phase to stable phases on annealing

The anneal-induced structural change in the metastable MC phase was examined for $Fe_{56}C_{14}V_{15}Cr_{15}$ alloy by X-ray diffraction and transmission electron microscopy. Fig. 15 shows the change in the X-ray diffraction pattern of melt-quenched $Fe_{56}C_{14}V_{15}Cr_{15}$ alloy with annealing temperature for 1 h. No distinct structural change in the MC phase is seen on annealing at temperatures below 873 K. At 973 K the diffraction peaks corresponding to ferrite (α) appear in addition to those of the VC phase, indicating the phase decomposition of MC to α + VC. A further rise of annealing temperature results in a progress of the splitting of the diffraction peaks of ferrite and MC, accompanied with a reduction of the half-width value of their peaks. Fig. 16 shows the variation of the lattice parameters of MC and ferrite as a function of annealing temperature. The lattice parameter of the MC phase is about 0.4024 nm in the melt-quenched state, remains unchanged up to about 873 K and increases rapidly to 0.4133 nm, which is close to the value ($\simeq$0.4144 nm) [8] of VC, in the narrow temperature range from 873 to 973 K, accompanied by the appearance of ferrite with a = 0.2873 nm. Considering the result that such a significant increase in the lattice parameter of MC phase occurs together with the appearance of ferrite, the large change in the lattice parameter of MC phase is interpreted as being due to the phase decomposition of the supersaturated MC = (Fe, V, Cr)C solid solution to equilibrium VC + α phases. The actually observed lattice parameter (0.2873 nm) of ferrite is slightly larger than that (0.2866 nm) of pure α-iron, being equal to that (0.2873 nm) of Fe–25 at % Cr [15] binary alloy. This indicates that the chromium atoms in the Fe–C–V–Cr alloy concentrate into ferrite phase rather than VC phase.

The decomposition behaviour of the metastable MC solid solution to VC + α(Fe, Cr) phases at temperatures above 973 K was also examined by TEM. Fig. 17 shows the microstructures of the MC phase in

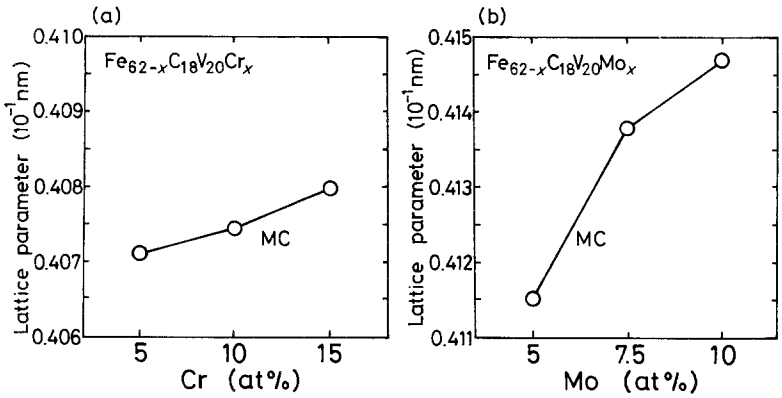

Figure 10 Variation of lattice parameter of (a) fcc (Fe, V, Cr)C phase in $Fe_{62-x}C_{18}V_{20}Cr_x$ alloys and (b) fcc (Fe, V, Mo)C phase in $Fe_{62-x}C_{18}V_{20}Mo_x$ alloys as a function of chromium or molybdenum content.

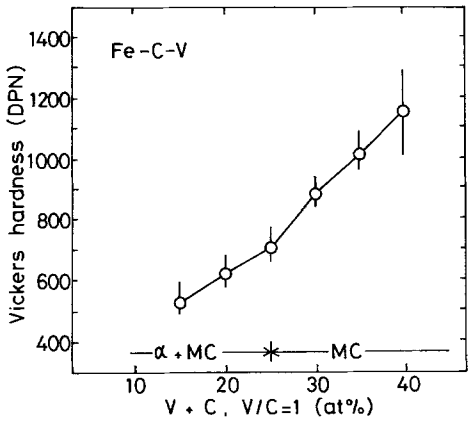

Figure 11 Change in Vickers hardness of the α + (Fe, V)C and (Fe, V)C phases in melt-quenched Fe–C–V alloys as a function of V + C (V/C = 1) content.

melt-quenched $Fe_{56}C_{14}V_{15}Cr_{15}$ alloy annealed for 1 h at (a) 973 K, (b) 1073 K, (c) 1173 K and (d) 1273 K. Similar to the results (Fig. 16) of examination by X-ray diffraction, any structural change in the MC phase is not seen on annealing at temperatures below 873 K. At 973 K, the phase decomposition of MC into α + VC becomes visible even in the conventional bright-field image. With further increase in annealing temperature, the recrystallization and grain growth of α-phase occurs more distinctly and the grain size increases significantly from about 0.1 μm at 973 K to about 1.5 μm at 1273 K as shown in Fig. 17a to d. On the other hand, the grain growth of VC carbide is more sluggish than that of α-phase and the particle diameter is as fine as about 0.4 μm even after annealing at 1273 K, as shown in Figs. 17 and 18. The decomposition behaviour of the metastable MC phase and the formation of the duplex structure including uniformly dispersed VC particles in an α matrix, were the same for all the MC phase alloys examined in the present work, except for the result that the matrix in Fe–C–V–5% Cr alloys annealed at 1273 K consists of lath martensite phase containing a high density of dislocations as exemplified for $Fe_{66}C_{14}V_{15}Cr_5$ in Fig. 19. The phase change from α to α'_L with decreasing chromium content is because annealing at 1273 K causes an austenitization of α-phase as is expected from the equilibrium diagram of Fe–Cr binary alloy [16] and the martensite transformation of the γ-phase occurs during air cooling from 1273 K. Here it is very

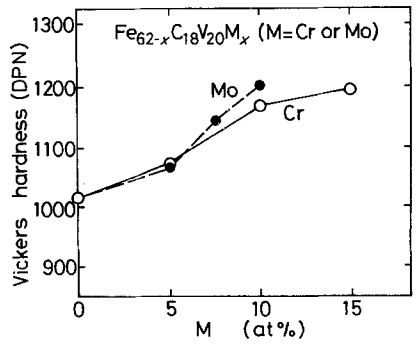

Figure 12 Change in Vickers hardness of the (Fe, V, Cr)C and (Fe, V, Mo)C phases in melt-quenched $Fe_{62-x}C_{18}V_{20}M_x$ (M = chromium or molybdenum) alloys as a function of chromium or molybdenum content.

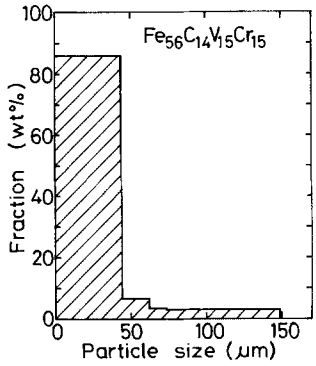

Figure 13 Particle size distribution for $Fe_{56}C_{14}V_{15}Cr_{15}$ powders produced by comminuting the melt-quenched ribbon for 30 min.

important to point out that the fine duplex structure obtained by annealing the metastable MC phase is in marked contrast to the structure of conventionally solidified Fe–C–V–Cr alloys containing primary VC carbides with diameters as large as about 15 to 35 μm. It is thus noted that the uniform dispersion of fine VC carbide is achieved even for Fe–C–V alloys containing a carbon content as much as about 14 to 18 at %. Such an unexpected and favourable result is thought to originate from the unique structural feature that the MC phase produced by melt quenching is a metastable iron-rich and carbon-poor solid solution without detectable segregation of alloy components.

3.6. Change in mechanical properties of the MC phase upon annealing

It was shown in Figs. 11 and 12 that the MC phase exhibits a Vickers hardness as high as about 700 to 1200 DPN, probably because of the solid solution hardening, the grain size refinement and the existence of a high density of internal faults. As shown in Figs. 16 and 17, the MC phase obtained by melt-quenching is a metastable phase and the subsequent annealing causes a structural change to α and VC in the temperature range from 873 to 973 K. Such a decomposition of the metastable MC solid solution is expected to result in a significant change in mechanical

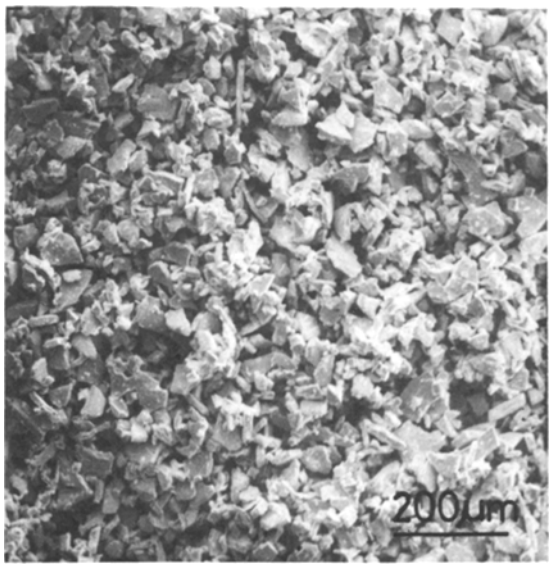

Figure 14 Scanning electron micrograph showing the $Fe_{56}C_{14}V_{15}Cr_{15}$ powders produced by comminuting the as-quenched ribbon.

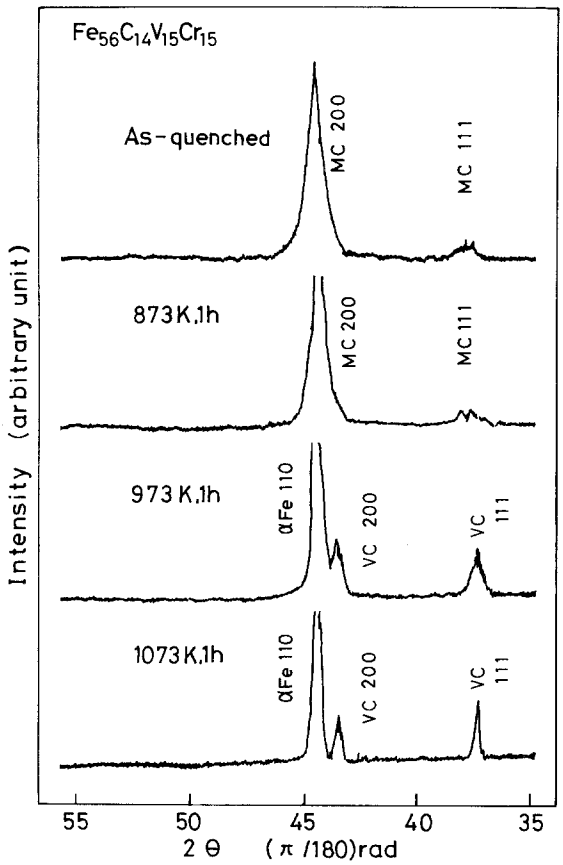

Figure 15 X-ray diffraction patterns showing the change in the MC phase in melt-quenched $Fe_{56}C_{14}V_{15}Cr_{15}$ alloy with annealing temperature.

properties such as hardness, tensile strength and ductility. Fig. 20 shows the change in Vickers hardness of the MC phase in $Fe_{56}C_{14}V_{15}Cr_{15}$ alloy as a function of annealing temperature. The hardness is about 1110 DPN in as-quenched state, remains constant up to 873 K and then decreases drastically to about 250 DPN in the temperature range from 900 to 1100 K. The temperature at which the MC phase begins to decompose into α + VC phases agrees well with the onset temperature of the decrease in hardness and hence the drastic decrease in hardness is concluded to originate from the structural change of the metastable MC phase to the stable duplex phases.

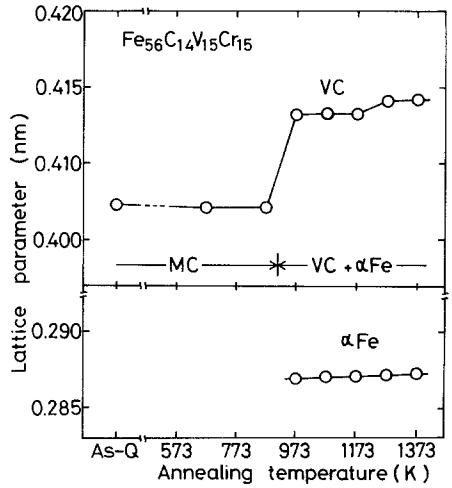

Figure 16 Variation of the lattice parameters of fcc MC phase and ferrite in melt-quenched $Fe_{56}C_{14}Cr_{15}V_{15}$ alloy as a function of annealing temperature.

Furthermore, the duplex ribbon samples produced upon annealing at 1273 K were found to exhibit good ductility which is shown by the 180° bending. This suggests the possibility that ductile high-carbon Fe–C–V–Cr alloys consisting of α + VC might be produced by annealing the melt-quenched MC phase at temperatures above 1173 K, even though the equilibrium phase alloys solidified at a conventional cooling rate are extremely brittle because of the appearance of primary VC carbide of large sizes, resulting from a carbon content as high as about 14 to 18 at %.

Fig. 21 shows the optical micrographs revealing an annealed (1273 K for 1 h) structure of melt-quenched $Fe_{56}C_{14}V_{15}Cr_{15}$ wires with MC single phase used for tensile property determination. A high density of fine VC carbides with an average size of about 0.5 μm are uniformly dispersed over the whole α matrix and no distinguishable difference in the duplex structure is seen in the cross and transverse sections. Fig. 22 plots the tensile fracture strength (σ_f), 0.2% proof stress ($\sigma_{0.2}$) and elongation (ε_p) as a function of chromium content for the $Fe_{71-x}C_{14}V_{15}Cr_x$ wires annealed at 1273 K for 1 h after melt quenching, along with the microstructures identified by X-ray diffraction. The $\sigma_{0.2}$ and σ_f are, respectively, 550 and 650 MPa at 5 at % Cr, remain almost unchanged in the range below about 10 at % Cr, but increase to about 1090 and 1125 MPa at 15 at % Cr. Unexpectedly, the change in ε_p with chromium content is very similar to those in $\sigma_{0.2}$ and σ_f, and the ε_p value increases from 0.3% at 5 at % Cr to 1.5% at 15 at % Cr. Thus, the $Fe_{56}C_{14}V_{15}Cr_{15}$ alloy consisting of α and VC exhibits rather high tensile strengths combined with an elongation of $\simeq$ 1.3% even at room temperature. Fig. 23 shows the fracture appearance of (a) $Fe_{66}C_{14}V_{15}Cr_5$ and (b) $Fe_{56}C_{14}V_{15}Cr_{15}$ wires fractured by uniaxial tensile stress. It does not look like highly embrittled behaviour, and reveals a rather high degree of ruggedness, suggesting that a rather large energy was spent for the nucleation and propagation of cracks. Additionally, it can be seen that the ruggedness is considerably larger for $Fe_{56}C_{14}V_{15}Cr_{15}$ than for $Fe_{66}C_{14}V_{15}Cr_5$, in accordance with the tendency of elongation shown in Fig. 22. The enhancements in $\sigma_{0.2}$, σ_f and ε_p for the alloy containing 15 at % Cr are thought to originate from the structural change in the matrix from α' to α. The above results enable us to expect that the application of an appropriate heat treatment to the metastable MC solid solution results in the formation of high-strength materials combined with rather good ductility, even though the carbon content is very high so as to be classified into so-called "cast iron". Furthermore, the fine duplex alloys are highly expected to exhibit large superplasticity at an appropriate strain rate at elevated temperatures, leading to an endowment of an easy workability into the ultra-high carbon alloy steels.

In conclusion, it may be mentioned that the metastable MC alloys found in Fe–C–V, Fe–C–V–Cr and Fe–C–V–Mo systems are attractive owing to the following advantages, e.g. (1) an easy formation of fine powders without detectable segregation of alloy components as a consequence of high hardness

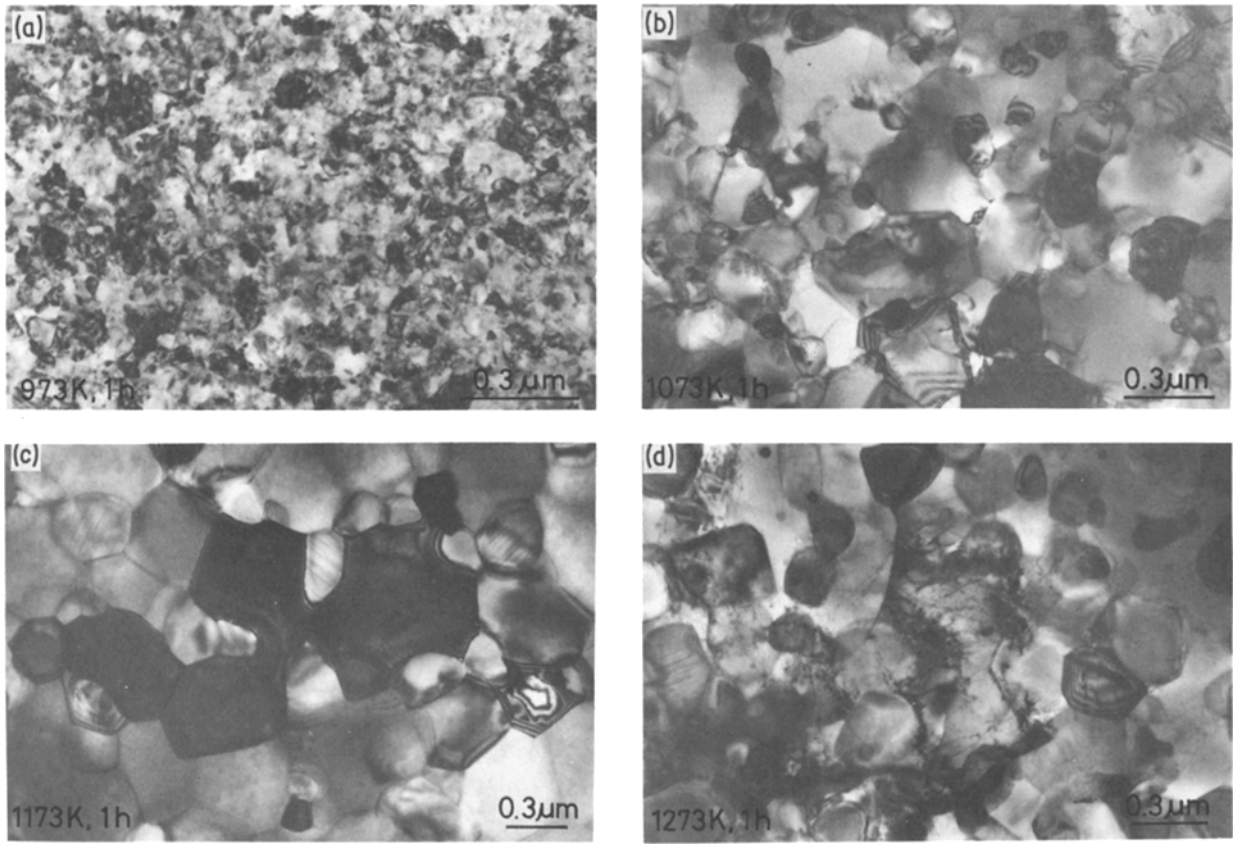

Figure 17 Transmission electron micrographs of the MC phase in melt-quenched $Fe_{56}C_{14}V_{15}Cr_{15}$ alloy annealed for 1 h at (a) 973 K, (b) 1073 K, (c) 1173 K and (d) 1273 K.

combined with highly brittle nature, (2) the MC phase decomposes into an aggregate of stable α-phase including a uniform dispersion of fine VC carbide, and (3) the high mechanical strengths and good ductility of the resultant duplex alloys.

4. Conclusions

The formation range, microstructure, mechanical properties and powder-forming tendency of metastable fcc MC single phase in Fe–C–V ternary and Fe–C–V–Cr and Fe–C–V–Mo quaternary alloys rapidly quenched from the melts and the anneal-induced changes in the microstructure and mechanical properties have been examined by means of X-ray diffraction, optical and transmission electron microscopies, Vickers hardness measurement, tensile test and hammer milling treatment, etc. The results obtained are summarized as follows.

1. The metastable fcc MC single phase is formed in the composition range 12 to 20 at % C and above 10 at % V for Fe–C–V alloys and below 12 at % C and above 19 at % V for Fe–18% C–V–Cr alloys. It is thus noticed that the formation of the MC phase is largely extended to the iron-rich and carbon-poor composition range. The MC single phase possesses ultra-fine grains of 0.1 to 0.2 μm and its lattice parameter increases with amounts of carbon, vanadium, chromium and molybdenum in the range 0.4048 to 0.4147 nm which are much smaller than that of VC carbide. The small values are due to the substitution of

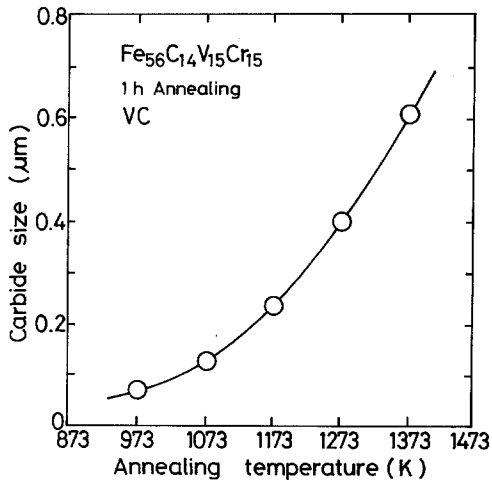

Figure 18 Particle size of VC carbide as a function of annealing temperature in $Fe_{56}C_{14}V_{15}Cr_{15}$ alloy annealed for 1 h after melt-quenching.

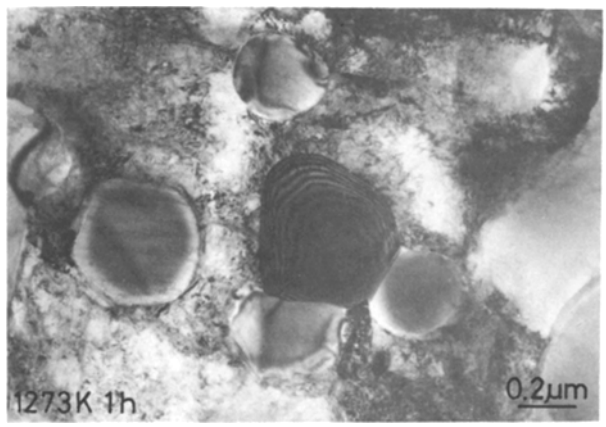

Figure 19 Transmission electron micrograph showing the microstructure of melt-quenched $Fe_{66}C_{14}V_{15}Cr_5$ alloy annealed for 1 h at 1273 K.

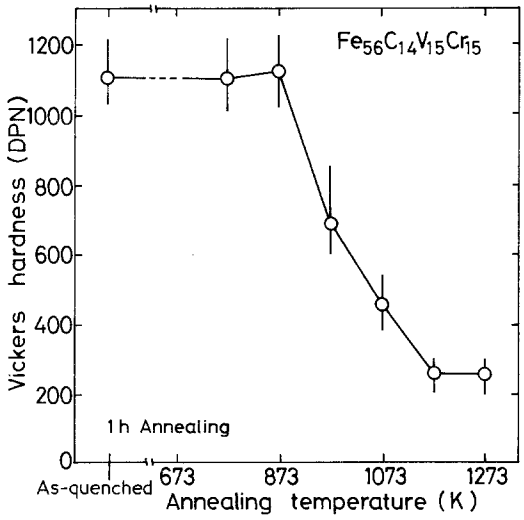

Figure 20 Vickers hardness of the MC phase in melt-quenched $Fe_{56}C_{14}V_{15}Cr_{15}$ alloy annealed for 1 h as a function of annealing temperature. The vertical bars represent the scatter in seven measurements.

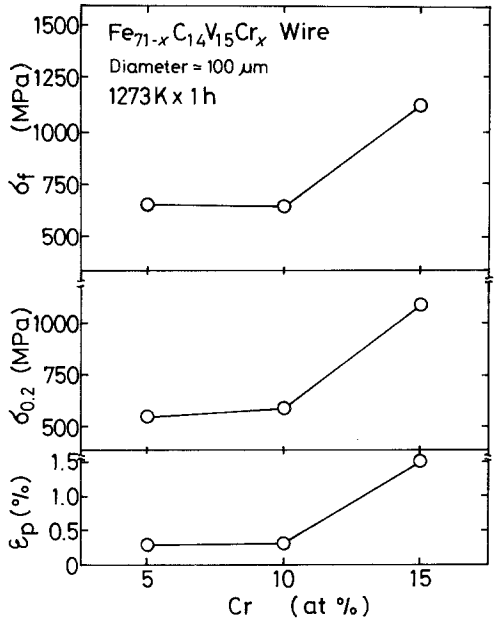

Figure 22 Changes in tensile fracture strength (σ_f), 0.2% proof stress ($\sigma_{0.2}$) and elongation (ε_p) as a function of chromium content for $Fe_{71-x}C_{14}V_{15}Cr_x$ wires annealed for 1 h at 1273 K after melt-quenching.

vanadium by iron and the carbon-poor concentration for the MC phase.

2. The hardness of the MC phase increases linearly with amounts of carbon, vanadium, chromium and molybdenum and reaches about 1200 DPN for $Fe_{47}C_{18}V_{20}Cr_{15}$ and $Fe_{52}C_{18}V_{20}Mo_{10}$. The high values are interpreted to be due to the solid solution hardening and the hardenings caused by the grain-size refinement and the introduction of a high density of internal faults.

3. As a consequence of the high hardness and extreme brittleness of the metastable MC phase, the application of hammer milling to the MC phase ribbons resulted in the formation of pulverized powders of a desirable size range below 44 μm and the powders had a morphology of irregularly shaped polygons which is suitable for subsequent consolidation processing.

4. The MC phase decomposes to α + VC during annealing for 1 h at temperatures below 873 and 973 K. A further annealing results in the spheroidization and growth of VC carbide as well as the recrystallization and grain growth of ferrite matrix, leading to the fine duplex structure with a uniformly dispersed VC carbide in ferrite.

5. The Fe–C–V, Fe–C–V–Cr and Fe–C–V–Mo alloys with the duplex α + VC structure, which were prepared by annealing the metastable MC phase for 1 h at 1273 K, exhibit an improved ductility and no

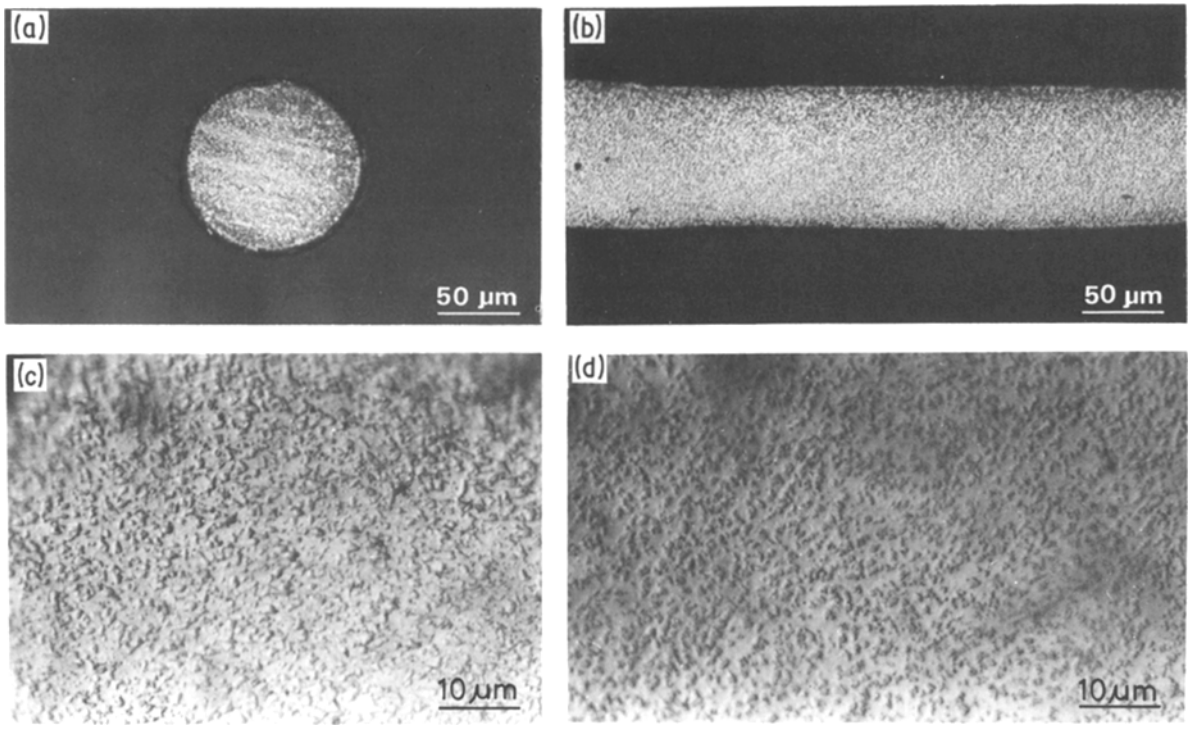

Figure 21 Optical micrographs of the $Fe_{56}C_{14}V_{15}Cr_{15}$ wire annealed for 1 h at 1273 K after melt-quenching. (a), (c) Cross-sections, (b), (d) longitudinal sections.

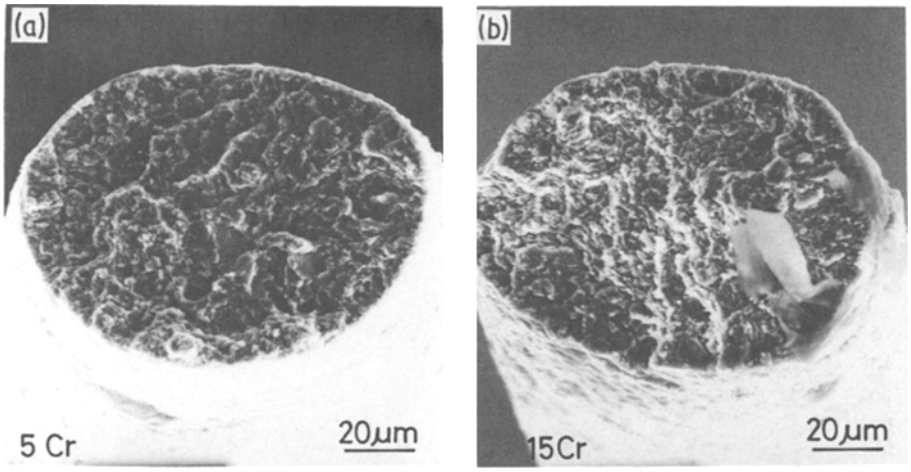

Figure 23 Scanning electron micrographs showing the tensile fracture appearance of (a) $Fe_{66}C_{14}V_{15}Cr_5$ and (b) $Fe_{56}C_{14}V_{15}Cr_{15}$ wires annealed for 1 h at 1273 K after melt-quenching.

crack is observed even after a closely contacted bending test in spite of carbon concentration as high as 14 at % and the $\sigma_{0.2}$, σ_f and ε_p are about 1090, 1125 MPa and 1.3%, respectively, for $Fe_{56}C_{14}V_{15}Cr_{15}$. The reason for such simultaneous achievement of rather high strengths and elongation is inferred to be due to the duplex structure of ferrite matrix including a uniform dispersion of fine VC carbide.

References

1. A. INOUE, T. MASUMOTO, S. ARAKAWA and T. IWADACHI, in "Rapidly Quenched Metals III", Vol. I, edited by B. Cantor (The Metals Society, London, 1978) p. 265.
2. A. INOUE, T. IWADACHI and T. MASUMOTO, *Trans. Jpn. Inst. Metals* **20** (1979) 76.
3. A. INOUE, T. IWADACHI, T. MINEMURA and T. MASUMOTO, *ibid.* **22** (1981) 197.
4. T. MINEMURA, A. INOUE, Y. KOJIMA and T. MASUMOTO, *Met. Trans.* **11A** (1980) 671.
5. T. MINEMURA, A. INOUE and T. MASUMOTO, *Trans. Iron Steel Inst. Jpn.* **21** (1981) 649.
6. T. MINEMURA, A. INOUE, Y. KOJIMA and T. MASUMOTO, *ibid.* **22** (1982) 934.
7. A. INOUE, T. MINEMURA, A. KITAMURA and T. MASUMOTO, *Met. Trans.* **12A** (1981) 1041.
8. H. SUZUKI, *Bull. Jpn. Inst. Metals* **5** (1955) 12.
9. C. E. DREMANN, in "Metals Handbook", 8th Edn. (ASM, Metals Park, Ohio, 1973) p. 415.
10. Y. HARAKAWA, A. INOUE and T. MASUMOTO, unpublished research (1983).
11. H. S. CHEN, *Acta Metall.* **22** (1974) 897.
12. D. TURNBULL, *J. Phys. C-4* **35** (1974) 1.
13. "Metals Databook", (Japan Institute of Metals, Maruzen, Tokyo 1983) p. 8.
14. *Idem*, p. 136.
15. W. B. PEARSON, in "A Handbook of Lattice Spacings and Structures of Metals and Alloys" (Pergamon Press, London, 1958) p. 532.
16. M. HANSEN, in "Constitution of Binary Alloys" (McGraw-Hill, New York, 1958) p. 525.

Received 30 April
and accepted 12 June 1985